Enhancing FSO Links Using Multi-HAPS and Opportunistic Relay Selection over IGGG Channels

Aishanee Chatterjee, Prashant Sharma, and Swaminathan R.
Department of Electrical Engineering, Indian Institute of Technology Indore,
Email: ms2504102001@iiti.ac.in, phd2301102004@iiti.ac.in, swamiramabadran@iiti.ac.in

***Abstract*—High-altitude platform station (HAPS)-assisted free-space optics (FSO) communication has emerged as a promising solution to enhance the coverage, flexibility, and resilience of existing network infrastructures through aerial relaying. By employing HAPS as relay nodes, the strict line-of-sight (LoS) constraints of conventional FSO links can be effectively alleviated. In this work, we investigate a multi-HAPS-based FSO communication system with decode-and-forward (DF) relaying, where opportunistic relay selection (ORS) is utilized to select the most suitable HAPS for data forwarding. The optical wireless channel is modeled using the doubly inverted Gamma–Gamma (IGGG) distribution, which jointly accounts for atmospheric turbulence, attenuation, and pointing errors. Closed-form analytical expressions are derived for outage probability (OP), while the average symbol error rate (ASER) and ergodic capacity (EC) are evaluated using efficient Gauss-Laguerre (GL) quadrature approximations. In addition, asymptotic analysis in the high signal-to-noise ratio (SNR) regime is performed to characterize the diversity gain of the proposed system. The analytical results are validated through Monte-Carlo simulations. Numerical results demonstrate the impact of relay selection strategies, turbulence conditions, and system parameters on system performance, providing useful insights into the reliability and diversity benefits of multi-HAPS-assisted FSO systems under realistic atmospheric environments.**

***Index Terms*—decode-and-forward (DF) relaying, doubly inverted gamma-gamma (IGGG) distribution, free space optics (FSO), high-altitude platform stations (HAPS), opportunistic relay selection (ORS).**

I. Introduction

Free-space optical (FSO) communication has emerged as a promising technology for next-generation wireless networks due to its capability to support gigabit-per-second data rates and its access to vast unlicensed optical spectrum compared to conventional radio-frequency (RF) systems. These advantages make FSO attractive for applications such as cellular backhaul, broadcasting, and video surveillance [1]. However, FSO links require strict line-of-sight (LoS) alignment and are sensitive to channel impairments including atmospheric turbulence, beam wander, pointing errors caused by transmitter–receiver misalignment, and path-loss-induced attenuation [2].

To improve link reliability under these impairments, non-terrestrial networks (NTNs) have gained significant attention. NTNs integrate space and aerial platforms such as satellites, uncrewed aerial vehicles (UAVs), and high-altitude platform stations (HAPS) to provide flexible relay-assisted communication infrastructures, enabling reliable LoS connectivity and extended coverage for 5G and beyond networks [3]. Among NTN platforms, HAPS are particularly attractive due to their stable operation in the stratosphere, which results in significantly lower platform jitter compared to UAVs and improves optical link stability. Their wide coverage, rapid deployability, and cost-effectiveness make them suitable for applications such as disaster recovery, emergency communication, remote connectivity, and environmental monitoring [4].

Several studies have investigated the use of HAPS to enhance the reliability and coverage of FSO-based communication systems. In [5], a HAPS relay is employed to improve the reliability of a hybrid FSO/RF link under Gamma-Gamma (GG) turbulence and pointing errors, where closed-form expressions for outage probability (OP) and average symbol error rate (ASER) are derived. In [6], the authors investigate the performance of a ground-to-satellite link employing multiple HAPS as relay nodes, where a partial relay selection (PRS) strategy is utilized considering Málaga turbulence with pointing errors. However, in this work, the multiple HAPS are deployed for communication with the satellite rather than with ground-based nodes. In [7], the authors analyze the performance of a dual-hop amplify-and-forward (AF) relaying system over GG turbulence channels, where a single HAPS is employed as the relay platform. In [8], serial relaying in multi-HAPS systems is investigated, where relay placement and the number of HAPS nodes are optimized under outdated channel state information (CSI), with FSO links for satellite–HAPS communication and mixed RF/FSO transmission for HAPS–ground links. Despite these advancements, most existing studies focus on single-HAPS systems or serial relaying, and do not fully exploit the spatial diversity offered by multi-HAPS networks to improve the coverage of ground-based nodes under realistic optical channel impairments. In particular, the combined impact of atmospheric turbulence, pointing errors, and atmospheric attenuation has not been thoroughly investigated within a multi-HAPS framework.

Motivated by the above limitations, this work investigates a multi-HAPS-assisted FSO communication system between two ground stations, where multiple HAPS act as relay nodes. To enhance link reliability, an opportunistic relay selection (ORS) strategy is employed to dynamically select the best relay, improving performance compared to conventional schemes. In contrast to existing studies [5]- [8], which rely on conventional turbulence models and relaying schemes, this work adopts the recently proposed doubly-inverted Gamma-Gamma (IGGG) distribution, a generalized model encompass-

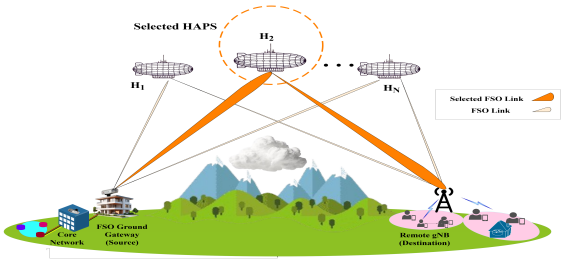

Fig. 1: System model of the Multiple HAPS-based FSO system

ing GG, $\mathcal{F}$, and lognormal distributions as special cases [9]. Consequently, it provides a suitable statistical model for FSO channels by characterizing small-, medium-, and large-scale irradiance fluctuations under diverse turbulence conditions, thereby enabling realistic performance evaluation when combined with non-zero boresight pointing errors and path loss.

The main contributions of this work are summarized as:

- A mathematical framework for ORS in a multi-HAPS-based FSO communication system is developed.
- The instantaneous signal-to-noise ratio (SNR) is statistically characterized through its probability density function (PDF) and cumulative distribution function (CDF).
- Based on the derived statistical expressions, a closed-form expression for OP is obtained, while the ASER and ergodic capacity (EC) are evaluated using Gauss-Laguerre (GL) quadrature approximations.
- In addition, asymptotic analysis is carried out to characterize the system behavior in the high-SNR regime. The performance is further compared with AF relaying [7] and PRS schemes, and all derived analytical expressions are validated through Monte-Carlo simulations.

II. System and Channel Models

We have considered an FSO communication system with multiple HAPS, denoted as H_j, $j{=}1,2,\ldots,N$, acting as decode-and-forward (DF) relay nodes to establish backhaul communication between a ground gateway source S and a remotely located gNB as destination D, where a direct LoS link is unavailable. The source is equipped with N aperture antennas, each directed toward a corresponding HAPS to establish individual FSO links. Each HAPS uses two antennas, one facing S and the other facing D. At S, subcarrier intensity modulation (SIM) combined with M-ary phase-shift keying (MPSK) is employed for optical transmission. At D, both heterodyne detection (HD) and direct detection (DD) techniques are considered for performance evaluation. Thus, the received electrical signal at D can be written as [9]

$$y(t) = \eta_D \left[h_j x(t)\right]^{\frac{r}{2}} + n_r(t), \tag{1}$$

where η_D is the photodiode responsivity at the receiver, h_j denotes the channel coefficient of the selected link, and $n_r(t)$ represents the additive white Gaussian noise (AWGN) with variance N_{or} (i.e., N_{o1} for HD and N_{o2} for DD). The transmitted optical signal $x(t)$ is be expressed as [9] $x(t){=}\rho_r\left[\Phi e(t)+1\right]$,where Φ denotes the modulation order and $e(t)$ represents the modulated baseband electrical signal. The parameter r denotes the detection technique, where $r{=}1$ and $r{=}2$ correspond to HD and DD, respectively. The parameter ρ_r is defined as $\rho_r{=}4P_tP_{LO}$ for $r{=}1$ (HD) and $\rho_r{=}P_t$ for $r{=}2$ (DD), where P_t is the transmitted optical power and P_{LO} denotes the local oscillator power. The combined channel gain of the FSO link between S and H_j or H_j and D is expressed as $h_j{=}h_j^p\,h_j^a\,h_j^l$, where $j{\in}\{SH_j,\,H_jD\}$. Here, h_j^p represents the non-zero boresight pointing error, h_j^a denotes the atmospheric turbulence modeled using the IGGG distribution, and h_j^l corresponds to the path loss component. The terms h_j^p and h_j^a are random variables (RVs), whereas h_j^l is considered a deterministic quantity. The path loss coefficient h_j^l is modeled using the Beer-Lambert Law as $h_j^l{=}e^{-\rho L_j}$, where ρ is the atmospheric attenuation coefficient that depends on the weather conditions and L_j is the propagation distance.

1) Atmospheric turbulence: The atmospheric turbulence-induced fading is modeled using IGGG distribution [9] as

$$f_{h_j^a}(h^a) = \frac{A_{\gamma_j}}{h^a}\, G_{1,2}^{2,1}\!\left(\frac{\alpha_j\beta_j h^a}{\lambda_j-1}\,\middle|\,\begin{matrix}1-\lambda_j\\ \alpha_j,\beta_j\end{matrix}\right) \tag{2}$$

where α_j, β_j and $\lambda_j{=}\alpha_j{-}2$ parameters determine the turbulence[1] of the j^{th} FSO link, $A_{\gamma_j}{=}\frac{1}{\Gamma(\alpha_j)\Gamma(\beta_j)\Gamma(\lambda_j)}$, where $\Gamma(.)$ is the Gamma integral function and $G_{.,.}^{.,.}(.)$ is the Meijer's G function [11].

2) Pointing error: Pointing errors occur due to the displacement of the optical beam from the receiver aperture, resulting in misalignment caused by (i) boresight displacement and (ii) random jitter. These displacements are modeled as independent Gaussian RVs along the horizontal and vertical axes. Consequently, the radial displacement follows a Beckmann distribution. Since the closed-form PDF of the Beckmann distribution is not available, it is commonly approximated by a modified Rayleigh distribution. Now, the PDF of the non-zero boresight pointing error h_j^p can be expressed as [6]

$$f_{h_j^p}(h^p) = \frac{g_j^2}{A_p^{g_j^2}}(h^p)^{(g_j^2-1)}, \qquad 0 \le h^p \le A_p, \tag{3}$$

where $g_j{=}\frac{w_{z_{eq}}}{2\sigma_{p_j}}$ denotes the pointing error coefficient, $w_{z_{eq}}$ is the equivalent beam waist at the receiver, σ_{p_j} represents the jitter variance, and A_{p_j} denotes the fraction of collected optical power at the detector aperture [6].

Using the PDFs in (2) and (3), and applying the product and transformation of RVs along with [11, Eq. (07.34.03.0605.01) and Eq. (07.34.21.0085.01)], the PDF of h_j is expressed as

$$f_{h_j}(h_j){=}\frac{g_j^2 A_{\gamma_j}}{h_j} G_{3,1}^{2,3}\!\left(\frac{\alpha_j\beta_j h_j}{(\lambda_j{-}1)h_j^l A_{p_j}}\,\middle|\,\begin{matrix}1{-}\lambda_j,\ 1+g_j^2\\ g_j^2,\ \alpha_j,\ \beta_j\end{matrix}\right). \tag{4}$$

For both IM/DD and HD technique, the instantaneous SNR γ_j of the j^{th} FSO link is written as $\gamma_j{=}\frac{\bar{\gamma}_j h_j^r}{[K_j h_j^l A_{p_j}]^r}$, and the average SNR is written as $\bar{\gamma}_j{=}\frac{4\eta_D^2(P_tP_{LO}Mh_j^lA_{p_j}K_j)^r}{N_{or}}$ for $r{=}1$

[1]The turbulence parameters α_j, β_j, and λ_j differ for uplink and downlink due to link geometry. In the uplink, a narrow beam interacts with large-scale eddies, causing beam wander, whereas in the downlink, beam expansion leads to an averaging effect where scintillation dominates and beam wander becomes negligible [5], [10].

and $\bar{\gamma}_j=\frac{\eta_D^2(P_t M h_j^l A_{p_j} K_j)^r}{N_{or}}$ for r=2, where $K_j=\frac{g_j^2}{g_j^2+1}$. The unified channel PDF of the instantaneous SNR in terms of the average SNR of the j^{th} FSO link is derived using (4), and the transformation of RVs as

$$f_{\gamma_j}(\gamma)=\frac{g_j^2 A_{\gamma_j}}{r\gamma_j} G_{2,3}^{3,1}\left(\frac{\alpha_j\beta_j K_j}{\lambda_j-1}\left(\frac{\gamma}{\bar{\gamma}_j}\right)^{\frac{1}{r}}\middle| \begin{matrix} 1-\lambda_j,\ g_j^2+1 \\ g_j^2,\ \alpha_j,\ \beta_j \end{matrix}\right). \quad (5)$$

Using (5) and [11, Eq. (07.34.21.0084.01)], the CDF of γ_j is obtained as

$$F_{\gamma_j}(\gamma)\approx g_j^2 A_{\gamma_j}\chi_j G_{2r+1,\,3r+1}^{3r,\,r+1}\left(D^r\frac{\gamma}{\bar{\gamma}_j}\middle| \begin{matrix} 1, K_{1,j}, K_{2,j} \\ K_{3,j}, 0 \end{matrix}\right), \quad (6)$$

where $\chi_j = \frac{r^{(\alpha_j+\beta_j+\lambda_j-2.5)}}{(2\pi)^{1.5(r-1)}}$, $D = \frac{\alpha_j\beta_j K_j}{(\lambda_j-1)r}$, $K_{1,j} = \left[\frac{1-\lambda_j}{r}, ..., \frac{1-\lambda_j+r-1}{r}\right]$, $K_{2,j} = \left[\frac{g_j^2+1}{r}, ..., \frac{1+g_j^2+r-1}{r}\right]$ and $K_{3,j} = \left[\frac{g_j^2}{r}, ..., \frac{g_j^2+r-1}{r}, \frac{\alpha_j}{r}, ..., \frac{\alpha_j+r-1}{r}, ..., \frac{\beta_j}{r}, ..., \frac{\beta_j+r-1}{r}\right]$.

The asymptotic CDF of FSO link $F_{\gamma_j}^{\infty}(\gamma)$ is calculated by considering $\bar{\gamma}_j\to\infty$ and subsequently employing [11, Eq.(07.34.06.0040.01)] on (6), $F_{\gamma_j}^{\infty}(\gamma)$ is obtained as

$$F_{\gamma_j}^{\infty}(\gamma_{th}) = \left(\frac{g_j^2 A_{\gamma_j} r^{(\alpha_j+\beta_j+\lambda_j-2.5)}}{(2\pi)^{1.5(r-1)}}\right)\times \sum_{k=1}^{3r}\frac{\prod_{\substack{l=1\\ l\neq k}}^{3r}\Gamma(b_{1,l}-b_{1,k})\ \prod_{l=1}^{r+1}\Gamma(1-a_{1,l}+b_{1,k})}{\prod_{l=r+2}^{2r+1}\Gamma(a_{1,l}-b_{1,k})\ \Gamma(1+b_{1,k})} B_1^{b_{1,k}} \quad (7)$$

where $a_{1,l}$=$\{1, K_{1,j}, K_{2,j}\}$, $b_{1,l}$=$\{K_{3,j}, 0\}$ and B_1=$\frac{D^r\gamma_{th}}{\bar{\gamma}_j}$.

III. Performance Analysis

In the ORS scheme, communication between S and D takes place in two time slots. In the first slot, S broadcasts its signal to all HAPS, while in the second slot, the HAPS forwards the decoded signal to D using the DF protocol. Thus, the optimal HAPS is selected based on the CSI of both hops. As per ORS strategy, the optimal HAPS among N available HAPs is selected based on the following rule:

$$\gamma_j^* = \arg\max_{j\in\{1,2,...,N\}}\{\gamma_j\}, \quad (8)$$

where γ_j denotes the instantaneous end-to-end SNR of the j^{th} FSO link between S and D, given by $\gamma_j=\min(\gamma_{SH_j}, \gamma_{H_jD})$, where γ_{SH_j} and γ_{H_jD} representing the instantaneous SNRs of the $S\to H_j$ and $H_j\to D$ links, respectively. Based on the above decision rule, we have obtained the exact and asymptotic expressions for performance metrics such as OP, ASER, and EC.

1) Outage Probability: In a multi-HAPS FSO system, an outage will occur, if the end-to-end instantaneous SNR of the selected link falls below a predefined threshold γ_{th}. Thus, the OP of the proposed system is written as

$$P_{out}^{j^*} = Pr(\gamma_j^*\le\gamma_{th}) = F_{\gamma_j^*}(\gamma_{th}), \quad (9)$$

where $F_{\gamma_j}(.)$ is the CDF of the instantaneous SNR of the selected HAPS-based link. As per the ORS strategy

$$F_{\gamma_j^*}(\gamma) = Pr\left\{\max_{j\epsilon 1,2,...,N}(\gamma_j)\le\gamma\right\} = \prod_{j=1}^{N}F_{\gamma_j}(\gamma). \quad (10)$$

Now, assuming each intermediate link (i.e., S→H$_j$ and H$_j$→D links) is independent of each other, $F_{\gamma_j}(\gamma)$ is written as

$$\begin{aligned} F_{\gamma_j}(\gamma) &= Pr\left\{\gamma_{SH_j}<\gamma\cup\gamma_{H_jD}<\gamma\right\} \\ &= F_{\gamma_{SH_j}}(\gamma) + F_{\gamma_{H_jD}}(\gamma) - F_{\gamma_{SH_j}}(\gamma)F_{\gamma_{H_jD}}(\gamma) \end{aligned} \quad (11)$$

where $F_{\gamma_{SH_j}}$ and $F_{\gamma_{H_jD}}$ are given by (6).

Without loss of generality, the S-to-H$_j$ and H$_j$-to-D links are assumed to experience independent and identically distributed (i.i.d.) fading for the subsequent derivation of asymptotic OP. Thus, $F_{\gamma_j}(\gamma)$ given in (11) is expressed as

$$F_{\gamma_j}(\gamma) = 2F_{\gamma_{SH_j}}(\gamma) - F_{\gamma_{SH_j}}^2(\gamma) \quad (12)$$

From (12), the end-to-end asymptotic CDF expression is written as

$$F_{\gamma_j}^{\infty}(\gamma) = \prod_{j=1}^{N}[2F_{\gamma_{SH_j}}^{\infty}(\gamma) - (F_{\gamma_{SH_j}}^{\infty})^2(\gamma)], \quad (13)$$

where $F_{\gamma_{SH_j}}^{\infty}(\cdot)$ is given by (7). By substituting (7) in (13), the expression for asymptotic OP is written as (14), which is given at the top of the next page.

2) Average SER: The ASER of the considered system is obtained using the derived end-to-end CDF expression and is written as [9]

$$P_e = \frac{b^a}{2\Gamma(a)}\int_0^{\infty}\frac{F_{\gamma_j^*}(\gamma)}{\gamma^{1-a}}e^{-b\gamma}d\gamma \quad (15)$$

where $F_{\gamma_j^*}(.)$ is given by (10), a=$\sin\left(\frac{\pi}{\Phi}\right)$ with Φ=2^n, while b=0.5 for n=1 and b=1 for $n\ge 2$, corresponding to MPSK modulation. The above integral in (15) is of the form $\int_0^{\infty}e^{-x}x^n f(x)dx$, which can be solved using the generalized Gauss-Laguerre (GL) quadrature technique [6] as

$$P_e \approx \frac{b^a}{2\Gamma(a)}\sum_{k=1}^{n}H_k F_{\gamma_j^*}(a_k) + E_n \quad (16)$$

where a_k represents the k^{th} root of the Laguerre polynomial of n^{th} order, H_k is the weight coefficient associated with the k^{th} root and E_n is the error term.

Similar to that of asymptotic OP, asymptotic ASER expression is written as

$$P_e^{\infty} \approx \frac{b^a}{2\Gamma(a)}\sum_{k=1}^{n}H_k F_{\gamma_j}^{\infty}(a_k) + E_n \quad (17)$$

where $F_{\gamma_j}^{\infty}(\cdot)$ is given by (13).

Remark 1: *From* (14) *and* (17) *it is observed that in the high-SNR region, OP and ASER decays with respect to average SNR as* $P_{out}^{\infty}\propto(\bar{\gamma}_j)^{-\mathcal{G}_d}$ *and* $P_e^{\infty}\propto(\bar{\gamma}_j)^{-\mathcal{G}_d}$, *respectively, where* $\mathcal{G}_d$=$\sum_{j=1}^{N}\min(\frac{g_j^2}{r}, \frac{\alpha_j}{r}, \frac{\beta_j}{r}, \frac{2g_j^2}{r}, \frac{2\alpha_j}{r}, \frac{2\beta_j}{r})$. *Now, from* (13) *it can be concluded that, at high SNR, the second-order term* $(F_{\gamma_{SH_j}}^{\infty}(\gamma))^2$ *becomes insignificant and only the first-order term* $F_{SH_j}^{\infty}(\gamma)$ *dominates. So, the net diversity order* $\mathcal{G}_d$=$\sum_{j=1}^{N}\min(\frac{g_j^2}{r}, \frac{\alpha_j}{r}, \frac{\beta_j}{r})$.*These results indicate that the achievable diversity gain of the system depends on atmospheric turbulence parameters* (α_j, β_j), *the pointing error severity coefficient* (g_j), *the detection scheme parameter* (r), *and the number of HAPS relays* (N) *but remains independent of modulation order* Φ.

$$P_{\text{out}}^{\infty} = \prod_{n=1}^{N} \left[1 - \left(1 - \frac{g_j^2 A_{\gamma_j} r^{(\alpha_j+\beta_j+\lambda_j-2.5)}}{(2\pi)^{1.5(r-1)}} \sum_{k=1}^{3r} \frac{\prod_{\substack{l=1 \\ l\neq k}}^{3r} \Gamma(b_{1,l}-b_{1,k}) \prod_{l=1}^{r+1} \Gamma(1-a_{1,l}+b_{1,k})}{\prod_{l=r+2}^{2r+1} \Gamma(a_{1,l}-b_{1,k}) \Gamma(1+b_{1,k})} B_1^{b_{1,k}} \right)^2 \right] \tag{14}$$

3) Ergodic Capacity: The normalized channel capacity, measured in (bit/s/Hz), represents the maximum achievable data rate that can be transmitted through the channel with a negligible error probability. We have calculated the EC of the proposed system by using the combined channel CDF as [9]

$$\bar{C} = \frac{1}{\ln 2} \int_0^{\infty} \frac{1 - F_{\gamma_j^*}(\gamma)}{1+\epsilon\gamma} \, d\gamma \tag{18}$$

where $F_{\gamma_j^*}(.)$ is given by (10), $\epsilon = 1$ for HD and $\frac{e}{2\pi}$ for DD, respectively. Now, due to mathematical complexity, we utilize the GL quadrature method [6, Eq. 31] to calculate the EC. After applying the GL approximation, (18) is written as

$$\bar{C} \approx \frac{1}{\ln 2} \sum_{k=1}^{K} H_k e^{a_k} \frac{1 - \prod_{j=1}^{N} F_{\gamma_j}(a_k)}{1+\epsilon\gamma_k} \tag{19}$$

IV. Numerical Results and Discussion

In this section, the analytical results derived in the previous sections are validated through Monte-Carlo simulations using 10^6 transmitted symbols. For simplicity, the zenith angles are assumed as θ_{SH_j}=θ_{H_jD}=80°, representing the propagation directions from the source to HAPS and from HAPS to the destination, respectively. Unless otherwise stated, system parameters are taken from well-published works in the literature [9], [6]. The FSO link operates at a wavelength of λ=1550 nm with transmit power P_t=30 dBm, a receiver aperture radius of 5 cm and an optical beam waist of 3 m [4]. Under strong turbulence conditions, the refractive index structure parameter is set to C_n^2=1.38 $\times 10^{-13}$ m$^{-2/3}$. The scattering parameters are α_{SH_j}=2.5, β_{SH_j}=2, λ_{SH_j}=1, α_{H_jD}=6.3, β_{H_jD}=2, and λ_{H_jD}=4.3. The HAPS and ground station heights are H_p=20 km and H_o=1 m, respectively, and remain fixed unless otherwise specified [4], [6], [9].

In Fig. 3, the OP of the proposed system is illustrated for different detection schemes r and varying numbers of HAPS N. It is observed that when N=4, the HD scheme (r=1) achieves an SNR gain of approximately 17.5 dB compared to the DD scheme (r=2) at an OP of 10^{-4}. This improvement is attributed to the coherent detection capability of HD, which provides higher sensitivity than DD. The impact of the number of HAPS on system performance is also examined. For an OP of 10^{-4}, a system with N=4 achieves an SNR gain of about 2.5 dB and 7.5 dB as compared to systems with N=3 and N=2, respectively, using the HD scheme. Furthermore, for N=2 and r=2, the OP values are 0.21 at 25 dB and 0.09 at 30 dB, yielding a diversity gain of G_d=0.71, which closely matches the value predicted by the asymptotic analysis in ***Remark 1***. Similarly, for N=4, the diversity gain is G_d=1.44 for r=2 and G_d=5.4 for r=1. These results indicate that increasing the number of HAPS improves the system diversity, while the HD technique maintains superior performance compared to DD.

In Fig. 3, the impact of the zenith angle ($\theta_{SH_j} = \theta_{H_jD} = [65°, 75°, 80°]$) and the pointing error severity (g_j=[1.8, 4]) on the OP of the proposed system is analyzed for $r = 2$. The results show that the system performance improves as the zenith angle decreases. Specifically, when θ_{SH_j}=θ_{H_jD}=65°, the system achieves noticeable SNR gains compared with the cases of 75° and 80° for the same outage value. This improvement occurs because a smaller zenith angle reduces the propagation path length and the Rytov variance, which increases the turbulence parameters α_j and β_j, thereby enhancing the diversity order G_d. For instance, as the zenith angle decreases from θ_{SH_j}=θ_{H_jD}=80° to 65°, the turbulence parameters increase from $[\alpha_j, \beta_j]$=[2.5, 2] to [4.6, 3], resulting in a significant increase in G_d from 1.2 to 4. Conversely, larger zenith angles increase the optical propagation distance, making the link more susceptible to free-space path loss, atmospheric turbulence, beam wander, and pointing errors, which degrades system performance. Fig. 3 also illustrates the effect of pointing error severity. For g_j=1.8 and g_j=4 with $\theta_{SH_j} = \theta_{H_jD} = 75°$ and r=2, the corresponding OP values at 25 dB are 5.6×10^{-4} and 3.4×10^{-4}, respectively. This improvement is attributed to better alignment conditions at higher g_j values, which reduce pointing error effects and enhance link stability. Consequently, G_d increases from 2.50 to 3.35 as g_j increases from 1.8 to 4, corresponding to an improvement of approximately 34%. These results further validate the claim in ***Remark 1*** that the diversity gain depends on pointing error severity and turbulence parameters.

In Fig. 4, the EC of the proposed system is evaluated by varying the number of HAPS N and the incoming optical beamwidth W_z. The results show that the EC increases with N due to the additional spatial diversity. At a received SNR of 25 dB, the EC values for N=2, 3, and 4 are approximately 4.65, 5.42, and 5.66 bits/s/Hz, respectively. Furthermore, the enhanced mobile broadband (eMBB) capacity requirement is satisfied at an SNR of about 26 dB for N=4 with W_z=3 m, whereas for N<4 and smaller beamwidths (W_z<3 m), the same requirement is achieved only at higher SNR values. In addition, since the pointing error coefficient is proportional to the beamwidth ($g_j \propto W_z$), reducing W_z increases the pointing error severity, leading to noticeable performance degradation.

In Fig. 5, the ASER performance is evaluated for different MPSK modulation schemes by varying the pointing error severity coefficient. As expected, the ASER decreases with increasing average SNR. To achieve an ASER of 0.05, BPSK provides SNR gains of approximately 6 dB and 11.5 dB compared to QPSK and 8-PSK, respectively, indicating that system performance degrades with increasing modulation order Φ . However, the asymptotic analysis shows that all modulation schemes achieve the same diversity gain, (i.e.,G_d=1.51), confirming that the diversity order is independent of Φ. Fur-

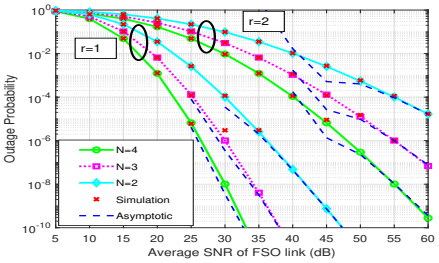

Fig. 2: OP by varying N and r.

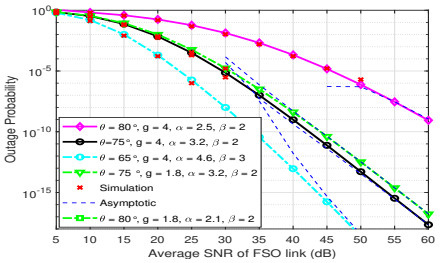

Fig. 3: OP for different values of θ and g.

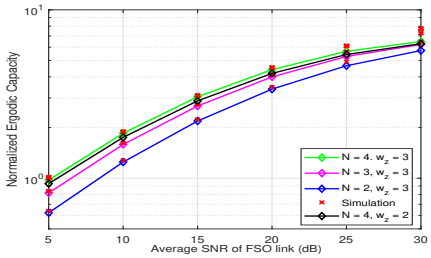

Fig. 4: EC for different values of N, W_z and r_d.

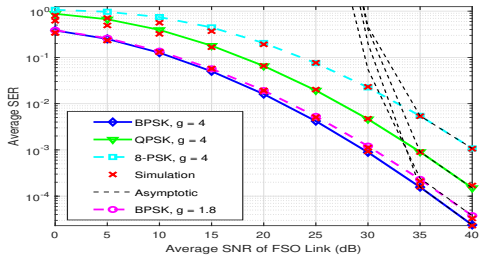

Fig. 5: ASER of the proposed system for MPSK under varying g_j.

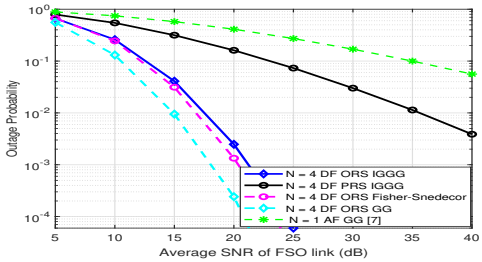

Fig. 6: OP comparison for different distributions and relay selection schemes.

thermore, Fig. 5 illustrates the impact of the pointing error coefficient g_j=$[1.8, 4]$ for the BPSK scheme. At an SNR of 25 dB, reducing g_j from 4 to 1.8 increases the ASER from 4.2×10^{-3} to 5.3×10^{-3}, accompanied by a reduction in diversity gain. These results show that the diversity gain depends on the pointing error coefficient but is independent of the modulation order, corroborating ***Remark 1***.

In Fig. 6, the OP of the proposed system (i.e., ORS) is compared with the PRS scheme for N=4 HAPS/relays and with the fixed gain AF relaying [7]. The results show that the ORS scheme consistently outperforms PRS. As ORS selects the relay based on the end-to-end instantaneous SNR, whereas the PRS scheme selects the relay solely based on the instantaneous SNR of the source-to-relay link. In Fig. 6 the proposed system outperforms the fixed-gain AF relaying scheme in [7]. Furthermore, it is shown that the IGGG turbulence model reduces to the GG and $\mathcal{F}$ distributions under specific parameter conditions. As discussed in [9], within the doubly stochastic framework, the IGGG distribution reduces to the GG model when $\alpha_j \to \infty$ (i.e., $\alpha_j \geq 14$) and to the $\mathcal{F}$ distribution when $\lambda_j \to \infty$ (i.e., $\lambda_j \geq 12$). Therefore, the GG and $\mathcal{F}$ distributions can be regarded as special cases of the IGGG model.

V. Conclusions

This article investigates the performance of a multi-HAPS-based FSO system for backhaul communication between a ground gateway and a remote gNB, employing ORS over IGGG turbulence channels. The analytical framework incorporates key channel impairments, including atmospheric turbulence, non-zero boresight pointing errors, and path loss, while considering both DD and HD detection schemes. Closed-form expressions for OP are derived, while the ASER and EC are evaluated using GL quadrature approximations and validated through Monte-Carlo simulations. Asymptotic analysis is further employed to characterize the system diversity gain. The results show that system performance improves with an increasing number of HAPS relays, whereas larger zenith angles, severe pointing errors, and smaller optical beamwidths degrade performance. Finally, the ORS scheme outperforms the PRS scheme, and comparison with GG and $\mathcal{F}$ models demonstrates the generality and versatility of the IGGG distribution in capturing weak-to-strong turbulence conditions.

VI. Acknowledgement

This research was supported by MeitY under the SwaYaan program (Ref. No. POC-Y3-01-IIT-ID-01) and the 5G Use Case Lab at IIT Indore, funded by the DoT, Govt. of India.

References

[1] M. A. Khalighi and M. Uysal, "Survey on free space optical communication: A communication theory perspective," *IEEE Commun. Surv. Tut.*, vol. 16, no. 4, pp. 2231–2258, 2014.

[2] H. Kaushal and G. Kaddoum, "Optical communication in space: Challenges and mitigation techniques," *IEEE Commun. Surv. Tut.*, vol. 19, no. 1, pp. 57–96, 2017.

[3] F. Rinaldi *et al.*, "Non-terrestrial networks in 5G & beyond: A survey," *IEEE Access*, vol. 8, pp. 165 178–165 200, 2020.

[4] Z. Lou *et al.*, "HAPS in the non-terrestrial network nexus: Prospective architectures and performance insights," *IEEE Wireless Commun.*, vol. 30, no. 6, pp. 52–58, 2023.

[5] S. R *et al.*, "HAPS-based relaying for integrated space–air–ground networks with hybrid FSO/RF communication: A performance analysis," *IEEE Trans. Aerosp. Electron. Syst.*, vol. 57, no. 3, pp. 1581–1599, 2021.

[6] D. Singh, R. Swaminathan, and A. T. Pham, "Multiple HAPS-based space-air-ground network with FSO communication: A performance analysis," *Appl. Opt.*, vol. 63, no. 9, pp. 2362–2375, Mar 2024.

[7] R. Deka *et al.*, "On the performance of a HAPS-assisted AF-based dual-hop FSO communication system," in *Proc. Int. Conf. Wireless Commun., Signal Process. Netw. (WiSPNET)*, 2022, pp. 13–18.

[8] S. E. Turk *et al.*, "Design of energy efficient multi-HAPS assisted hybrid RF/FSO satellite communication systems with optimal placement," *IEEE Trans. Green Commun. Netw.*, vol. 9, no. 3, pp. 910–922, 2025.

[9] P. Sharma, S. R., and A. T. Pham, "Comprehensive performance analysis of UAV-assisted mixed FSO-RF communication system with nonlinear energy harvesting," *IEEE Trans. Veh. Technol.*, pp. 1–16, 2026.

[10] L. C. Andrews and R. L. Phillips, *Laser Beam Propagation Through Random Media*, 2nd ed. Bellingham, WA, USA: SPIE Press, 2005.

[11] Wolfram Research, Inc., "Meijer G," https://reference.wolfram.com/language/ref/MeijerG.html, 2026, accessed: Mar. 6, 2026.